Evaluation of the Moderate-Resolution Imaging Spectroradiometer (MODIS) retrievals of dust aerosol over the ocean during PRIDE

Robert C. Levy,[1,2] Lorraine A. Remer,[2] Didier Tanré,[3] Yoram J. Kaufman,[2] Charles Ichoku,[1,2] Brent N. Holben,[4] John M. Livingston,[5] Philip B. Russell,[6] and Hal Maring[7]

Received 18 April 2002; revised 13 August 2002; accepted 14 August 2002; published 23 July 2003.

[1] The Puerto Rico Dust Experiment (PRIDE) took place in Roosevelt Roads, Puerto Rico from 26 June to 24 July 2000 to study the radiative and physical properties of African dust aerosol transported into the region. PRIDE had the unique distinction of being the first major field experiment to allow direct comparison of aerosol retrievals from the Moderate Imaging Spectroradiometer (MODIS) with Sun photometer and in situ aerosol measurements. Over the ocean the MODIS algorithm retrieves aerosol optical depth (AOD) as well as information about the aerosols' size distribution. During PRIDE, AODs derived by MODIS in the red wavelengths (0.66 μm) compare closely with Sun photometers. However, MODIS-derived AODs are too large in the blue and green wavelengths (0.47 and 0.55 μm) and too small in the near infrared (0.87 μm). This error in AOD spectral dependence results in retrieved particle size distributions that are small compared to in situ measurements and smaller still when compared to Sun photometer sky radiance inversions. The differences in size distributions may be, in part, associated with MODIS' simplification of dust as spherical particles. Analysis of this PRIDE data set is a first step toward derivation of realistic models for future MODIS retrievals. *INDEX TERMS:* 0305 Atmospheric Composition and Structure: Aerosols and particles (0345, 4801); 0345 Atmospheric Composition and Structure: Pollution—urban and regional (0305); 0360 Atmospheric Composition and Structure: Transmission and scattering of radiation; 1640 Global Change: Remote sensing; 4801 Oceanography: Biological and Chemical: Aerosols (0305); *KEYWORDS:* Saharan dust, aerosol, MODIS, PRIDE, Puerto Rico, Sun photometer

Citation: Levy, R. C., L. A. Remer, D. Tanré, Y. J. Kaufman, C. Ichoku, B. N. Holben, J. M. Livingston, P. B. Russell, and H. Maring, Evaluation of the Moderate-Resolution Imaging Spectroradiometer (MODIS) retrievals of dust aerosol over the ocean during PRIDE, *J. Geophys. Res.*, *108*(D19), 8594, doi:10.1029/2002JD002460, 2003.

1. Introduction

[2] Mineral dust aerosols are produced mainly by wind erosion of desert soils, and are a significant component of tropospheric aerosols [*Prospero*, 1996; *Chiapello et al.*, 1999]. These aerosols are lifted by the wind, raised to high altitudes by convection, and may be transported over long distances from their sources [*Ginoux et al.*, 2001; *Li-Jones and Prospero*, 1998; *Formenti et al.*, 2001; *Smirnov et al.*, 2000b]. They influence the optical properties of the Earth's atmosphere and climate through the scattering and absorption of sunlight [*Tanré et al.*, 2001], in turn influencing local and global atmospheric dynamics [*Alpert et al.*, 1998; *Miller and Tegen*, 1998]. As for other effects, dust aerosol may influence photochemical processes [*Dickerson et al.*, 1997], contribute to cloud condensation nuclei [*Levin and Ganor*, 1996], or act to suppress precipitation [*Rosenfeld et al.*, 2001]. Dust is deposited into the ocean [*Gao et al.*, 2001], and is related to the biological productivity of a basin. Mineral dust in large quantities affects visibility, and may have adverse influences on human health [*Prospero*, 1999], and upon animal populations [*Stallard*, 2001]. Recent studies, mentioned by *Sokolik et al.* [2001], suggest that some change in dust production may be caused by anthropogenic activities [*Tegen et al.*, 1996; *Tegen and Fung*, 1995], though satellite data analysis indicates dominance of sources in scarcely populated regions [*Prospero et al.*, 2002].

[3] A major source region for mineral dust is the combined Sahara and Sahel areas of North Africa [*Prospero*, 1996; *Moulin et al.*, 1997; *Johansen et al.*, 2000]. This source is active nearly all year, with plumes flowing across the Atlantic toward the Caribbean and the Americas, especially during the summer months [*Prospero*, 1996; *Higurashi et al.*, 2000].

[1]Science Systems and Applications Inc., Lanham, Maryland, USA.
[2]Laboratory for Atmospheres, NASA Goddard Space Flight Center, Greenbelt, Maryland, USA.
[3]Laboratoire d'Optique Atmospherique, CNRS, Universite de Sciences et Techniques de Lille, Villeneuve d'Ascq, France.
[4]Laboratory for Terrestrial Physics, NASA Goddard Space Flight Center, Greenbelt, Maryland, USA.
[5]SRI International, Menlo Park, California, USA.
[6]NASA Ames Research Center, Moffett Field, California, USA.
[7]Rosenstiel School of Marine and Atmospheric Science, University of Miami, Miami, Florida, USA.

0148-0227/03/2002JD002460$09.00

These plumes have been well documented by satellite sensors such as the Total Ozone Mapping Spectrometer (TOMS) [*Herman et al.*, 1997; *Chiapello et al.*, 1999] and the advanced very high resolution radiometer (AVHRR) [*Husar et al.*, 1997; *Higurashi et al.*, 2000]. Ground based in situ instruments and Sun photometers have also observed dust in the Caribbean, at sites such as Barbados [*Prospero*, 1996; *Smirnov et al.*, 2000b].

[4] For some dusty regions of the world, satellite observations have been linked to Sun photometer data in the works of *Higurashi et al.* [2000] and *Livingston et al.* [2000] (using AVHRR data), *Tanré et al.* [2001] (using Thematic Mapper data.), and *Moulin et al.* [1997] (using Meteosat data). Specifically, in the Caribbean, satellite retrievals have been compared with in situ measurements by works such as *Husar et al.* [1997] and *Chiapello et al.* [1999]. These studies have shown that satellite retrievals are a promising method for identifying dust and retrieving its properties.

[5] As part of the NASA's Earth Observing System (EOS), the Terra satellite was launched in December 1999. Aboard Terra, the MODerate resolution Imaging Spectrometer (MODIS) [*Salmonson et al.*, 1989; *King et al.*, 1992] is a state-of-the-art instrument that monitors the globe with a wide spectral range, near daily global coverage, and fine spatial resolution. MODIS' new capabilities enable aerosol retrievals over both land [*Kaufman et al.*, 1997] and ocean [*Tanré et al.*, 1997]. Over the ocean, MODIS is routinely retrieving a suite of aerosol properties including spectral optical depths and particle size distributions [*Tanré et al.*, 1997]. This aerosol algorithm has been validated under a variety of conditions [*Remer et al.*, 2002], but no evaluation has been made specifically for dust regimes.

[6] Retrieving dust aerosol properties from satellite may prove to be particularly challenging, mainly due to the nonspherical shape of dust particles. Microscopic analyses of dust particles show that they are irregular in shape rather than spherical [*Koren et al.*, 2001]. However, the dust optical properties for MODIS, similarly to previous satellite missions, are modeled by assuming that the particles are spherical [*Tanré et al.*, 1997]. Investigators such as *Mischenko and Travis* [1997] showed that nonsphericity may have large effects on the scattering optical properties of the aerosol, especially at large scattering angles (greater than 120°) that would be seen by MODIS.

[7] An opportunity for dust validation arose with the Puerto RIco Dust Experiment (PRIDE) [*Reid et al.*, 2000, 2003]. Held from 26 June to 24 July 2000, PRIDE was operated from Roosevelt Roads, Puerto Rico, and was designed to study the African dust aerosol transported into Puerto Rico. For MODIS, PRIDE had the unique distinction of being the first major field experiment to allow direct comparison of its aerosol retrievals to field measurements.

[8] In this study, we report on the evaluation of the MODIS aerosol retrievals over the ocean during PRIDE, using Sun photometer and in situ observations. In section 2, we outline the theoretical and operational use of the MODIS aerosol over ocean algorithm. Section 3 describes each instrument used to validate the MODIS retrievals, and the data taken during PRIDE. In section 4, we show the comparisons of MODIS and validation data, and in section 5, we discuss how these comparisons should be used as a basis for new science on dust aerosol.

2. MODIS Aerosol Retrieval

[9] The Moderate Imaging Spectroradiometer (MODIS) is a new instrument aboard the Earth Observing System (EOS) satellites [*Salmonson et al.*, 1989; *King et al.*, 1992]. MODIS performs measurements at 36 channels in the solar and infrared regions (0.415 to 14.235 μm), with resolutions of 250 m, 500 m, or 1 km, depending on the wavelength. At a nominal altitude of about 700 km, MODIS observes a swath about 2300 km wide. The first MODIS instrument was launched with the Terra satellite in December, 1999, which has a Sun-synchronous orbit that passes southward over the equator at 10:30 AM local (solar) time. Aboard Terra, MODIS provides nearly global coverage each day. MODIS's wide spectral range and fine spatial resolution, coupled with its broad swath over the Earth's surface, make it suitable for monitoring events on short term local time and spatial scales, as well as for global and long term scales.

2.1. Theoretical Description of the Retrieval Algorithm

[10] *Tanré et al.* [1997] details the strategy for using MODIS to retrieve aerosol properties over the ocean. Observed top of the atmosphere (TOA) reflectances at six wavelengths (0.55, 0.66, 0.87, 1.24, 1.64 and 2.13 μm) are compared with a lookup-table of precomputed reflectance for an array of angles, size distributions and optical depths. The modeled reflectance with the smallest difference from the observed reflectance is retrieved from the look up table. This best fit reflectance is associated with a corresponding set of aerosol properties, which are considered to be the retrieved products. Results for the aerosol retrieval are reported at the six wavelengths mentioned above, plus at 0.47 μm, which is extrapolated from the lookup table.

[11] The reflectances in the lookup table are computed from aerosol models that represent the aerosol properties of a vertical column. Currently, nine tropospheric aerosol models are used, including four ''fine'' mode models (accumulation mode: dominated by chemical and combustion processes) and five ''coarse'' mode models (dominated by maritime particles and dust). The optical models are described in Tables 1a and 1b. The current lookup tables were updated from those described by *Tanré et al.* [1997], the main difference being the use of new ''dust-like'' particle models (modes 8 and 9 in Table 1b). Their scattering and absorption properties were derived from a combination of AERONET data and LANDSAT Thematic Mapper (TM) image analysis [*Tanré et al.*, 2001; *Kaufman et al.*, 2001].

[12] The modeled satellite signal is assumed to be a combination of radiation from the atmosphere and from the surface. The atmospheric contribution includes multiple scattering by gas and aerosol, as well as reflection of the atmosphere by the sea surface. The ocean surface calculation includes Sun glint reflection off the surface waves [*Cox and Munk*, 1954], reflection by whitecaps [*Koepke*, 1984] and Lambertian reflectance from underwater scattering (sediments, chlorophyll, etc). For the current version of the lookup table, reflectances have been calculated using a surface wind of 6.0 m/s. Zero water leaving radiance is

Table 1a. Refractive Indices, Median, Standard Deviation, and Effective Radius for Small Mode Particles Used in the MODIS Lookup Table

S	λ = 0.47 –> 0.86 μm	λ = 1.24 μm	λ = 1.64 μm	λ = 2.13 μm	r_g	σ	Reff	Comments
1	1.45-0.0035i	1.45-0.0035i	1.43-0.01i	1.40-0.005i	0.07	0.40	0.10	wet water soluble type
2	1.45-0.0035i	1.45-0.0035i	1.43-0.01i	1.40-0.005i	0.06	0.60	0.15	wet water soluble type
3	1.40-0.0020i	1.40-0.0020i	1.39-0.005i	1.36-0.003i	0.08	0.60	0.20	water soluble with humidity
4	1.40-0.0020i	1.40-0.0020i	1.39-0.005i	1.36-0.003i	0.10	0.60	0.25	water soluble with humidity

assumed at all six compared wavelengths, except for at 0.55 μm, where a fixed reflectance of 0.005 is used. Because the reflectance in the blue is highly related to undetermined underwater chlorophyll and sediments, the water leaving radiance at 0.47 μm is not specified in the lookup table.

[13] Using the radiative transfer code developed by *Ahmad and Fraser* [1981], spectral reflectances were computed for each of the nine aerosol models. Five values of aerosol columnar optical depth, τ_a, (total aerosol loading) at 0.55 μm are considered for each mode, ranging from a pure molecular (Rayleigh) atmosphere (τ_a = 0.0) to a highly turbid atmosphere (τ_a = 2.0), with intermediate values of 0.2, 0.5 and 1.0. For each model and aerosol optical depth at 0.55 μm, the associated aerosol optical depths are stored for the other six wavelengths, including the blue (at 0.47 μm). Computations are performed for combinations of 9 solar zenith angles, 16 satellite zenith angles and 16 relative Sun/satellite azimuth angles (2304 total combinations).

[14] To perform the aerosol retrieval, we use the method discussed by *Tanré et al.* [1997]. The multiple scattering radiance from two lognormal modes (we assume one small, one large) can be approximated by the weighted average of the two modes, calculated for the same optical thickness [*Tanré et al.*, 1996; *Gordon*, 1997]. Let us assume that the total reflectance measured at a wavelength channel λ, ρ_λ^m, (superscript "m" denotes "measured") at the satellite level is:

$$\rho_\lambda^m = \eta\rho_\lambda^s + (1-\eta)\rho_\lambda^l, \tag{1}$$

where ρ_λ^s and ρ_λ^l are the reflectances of the small (s) and large (l) modes, respectively, and η is the ratio of the reflectance contribution of the small mode as compared to the total (defined at 0.55 μm). Note that these reflectances must include contributions from the surface and Rayleigh scattering.

[15] Given one of the 20 combinations of small and large modes, we compute the expected reflectance by interpolating to the exact Sun/satellite geometry, for each of the aerosol optical depths in the table. Using the 0.87 μm channel, we obtain a first-guess AOD for the combination by comparing to the observed reflectance, and then derive the optical thickness at the other wavelengths. Assuming the single scattering approximation, the reflectance small mode ratio, η, can also be thought of as the optical depth small mode ratio:

$$\eta = \tau^S/\tau \tag{2}$$

If we denote the calculated reflectance at channel λ by $\rho_\lambda^{c,sl}$, (where sl represents the combination of small and large modes) and the measured reflectance by ρ_λ^m, then the relative error between the two, ε_λ^{sl}, is given by:

$$\varepsilon_\lambda^{sl} = \frac{\rho_\lambda^m - \rho_\lambda^{c,sl}}{\rho_\lambda^{c,sl} + 0.01}, \tag{3}$$

where the constant 0.01 is a small residual used to prevent division by zero and to minimize uncertainty [*Tanré et al*, 1997]. The total root-mean square (rms) relative error for all wavelengths, ε^{sl}, is thus given by:

$$\varepsilon^{sl} = \sqrt{\frac{1}{n}\sum_{\lambda=1}^{n}\left(\varepsilon_\lambda^{sl}\right)^2}, \tag{4}$$

where the summation is over the six nonblue (0.55, 0.66, 0.87, 1.24, 1.64 and 2.13 μm) wavelengths. Whichever ratio η, of the combination of modes, *sl*, gives the smallest total relative error is considered the "best" solution. In practice, we often use the average for the three combinations with the smallest error.

[16] Once the spectral optical depths, the models, and the small mode ratio are chosen, they can be matched to aerosol physical properties through the lookup table. For example, the number size distributions for each mode are retrieved

Table 1b. Refractive Indices, Median, Standard Deviation, and Effective Radius for Large Mode Particles Used in the MODIS Lookup TABLE

B	λ = 0.47 –> 0.86 μm	λ = 1.24 μm	λ = 1.64 μm	1λ = 2.13 μm	r_g	σ	Reff	Comments
5	1.45-0.0035i	1.45-0.0035i	1.43-0.0035i	1.43-0.0035i	0.40	0.60	0.98	wet sea-salt type
6	1.45-0.0035i	1.45-0.0035i	1.43-0.0035i	1.43-0.0035i	0.60	0.60	1.48	wet sea-salt type
7	1.45-0.0035i	1.45-0.0035i	1.43-0.0035i	1.43-0.0035i	0.80	0.60	1.98	wet sea-salt type
8	1.53-0.003i (0.47) 1.53-0.001i (0.55) 1.53-0.000i (0.66) 1.53-0.000i (0.86)	1.46-0.000i	1.46-0.001i	1.46-0.000i	0.60	0.60	1.48	dust-like type
9	1.53-0.003i (0.47) 1.53-0.001i (0.55) 1.53-0.000i (0.66) 1.53-0.000i (0.86)	1.46-0.000i	1.46-0.001i	1.46-0.000i	0.50	0.80	2.50	dust-like type

Table 2. MODIS Overpass Parameters for Roosevelt Roads, Puerto Rico, During PRIDE[a]

Date	DOY	Time	Solar_Zen	Sensor_Zen	Relative_Azm	Scat_Angle	Glint_Angle	Glint/No Glint
26 June 2000	178	14:58	20.89	39.75	25.11	157.63	59.21	no glint
27 June 2000	179	15:41	12.08	45.05	148.31	124.39	35.23	glint
28 June 2000	180	14:46	23.72	54.76	22.90	146.19	76.96	no glint
29 June 2000	181	15:29	14.13	25.18	147.76	142.16	15.11	glint
30 June 2000	182	14:34	26.59	64.95	20.98	139.22	90.00	no glint
1 July 2000	183	15:16	16.91	2.05	32.49	164.78	18.67	glint
2 July 2000	184	15:59	7.92	63.08	129.94	111.69	58.18	no glint
3 July 2000	185	15:04	19.77	29.38	25.02	166.02	47.96	no glint
4 July 2000	186	15:47	10.34	52.09	141.33	119.60	44.36	no glint
5 July 2000	187	14:52	22.51	47.56	22.44	152.20	68.76	no glint
6 July 2000	188	15:34	12.90	36.37	148.01	132.27	26.21	glint
7 July 2000	189	14:39	25.38	60.22	20.16	142.94	84.29	no glint
8 July 2000	190	15:22	15.64	12.40	153.34	152.72	7.14	glint
9 July 2000	191	16:04	7.79	68.20	123.00	107.42	64.12	no glint
10 July 2000	192	15:10	18.50	16.53	24.11	172.54	34.24	glint
11 July 2000	193	15:52	8.93	58.50	141.76	114.34	51.68	no glint
12 July 2000	194	14:57	21.37	39.75	20.92	159.01	60.11	no glint
13 July 2000	195	15:40	11.56	45.05	150.25	124.68	35.38	glint
14 July 2000	196	14:45	24.16	54.75	18.57	147.50	77.89	no glint
15 July 2000	197	15:28	14.28	25.18	155.45	141.40	13.48	glint
16 July 2000	198	14:33	27.01	64.92	16.63	140.51	90.94	no glint
17 July 2000	199	15:15	17.10	2.04	25.28	164.72	18.96	glint
18 July 2000	200	15:58	7.40	63.05	146.07	110.74	57.00	no glint
19 July 2000	201	15:02	20.02	29.37	18.50	167.97	48.73	no glint
20 July 2000	202	15:46	10.14	52.08	154.13	118.69	43.12	no glint
21 July 2000	203	14:50	22.94	48.56	15.97	152.92	70.82	no glint
22 July 2000	204	15:33	12.91	35.41	159.70	132.30	23.67	glint
23 July 2000	205	14:38	25.67	60.19	14.28	144.32	85.19	no glint
24 July 2000	206	15:21	15.71	11.49	163.60	153.08	5.68	glint
25 July 2000	207	16:03	8.24	67.50	123.06	107.85	63.19	no glint
26 July 2000	208	15:09	18.66	17.43	14.96	175.22	35.77	glint

[a]DOY is the day of year, or the Julian date. The columns marked "Solar_Zen," "Sensor_Zen," Relative_Azm," and "Scat_Angle" denote the solar zenith angle, sensor zenith angle, relative azimuth (solar/sensor) angle, and the scattering angle, respectively.

and then combined to compute the effective radius Reff of the particle population, defined as:

$$Reff = \frac{\int_{r=0}^{r=\infty} r^3 \frac{dN(r)}{d\ln r} d\ln r}{\int_{r=0}^{r=\infty} r^2 \frac{dN(r)}{d\ln r} d\ln r}, \quad (5)$$

where r is the radius.

2.2. Retrieval Algorithm in Operation

[17] Proper preparation of the MODIS input is necessary for producing valid aerosol retrievals. Using a separately produced geo-location file, the MODIS scenes are separated into land and ocean pixels. At the same time, the MODIS reflectance data are binned into 10 km by 10 km boxes (i.e., 20 by 20 pixel boxes for the 500 m channels of 0.66 and 0.87 μm, and 40 by 40 pixel boxes for the 250 m channels of 0.47, 0.55, 1.24, 1.64 and 2.13 μm). A combination of reflectance thresholds and variability tests [*Martins et al.*, 2002] yields a cloud mask and quality screened data. Using the reflectance at 0.87 μm, we remove the brightest 25% and darkest 25% of the remaining (nonscreened) pixels in each 10 km x 10 km box, in order to minimize contamination arising from inhomogeneous surfaces and subpixel clouds. Averages and standard deviations of the remaining pixels are stored.

[18] Before doing the actual aerosol retrieval, we perform a number of tests on the reflectance data; for example, we ensure that all reflectance values are greater than or equal to the Rayleigh value. Additionally, we compute the glint angle, which denotes the angle of reflection, compared with the specular reflection angle. The glint angle is defined as:

$$\Theta_{\text{glint}} = \cos^{-1}\left((\cos\theta_S \cos\theta_V) - (\sin\theta_S \sin\theta_V \cos\phi)\right), \quad (6)$$

where θ_s, θ_v, and ϕ are the solar zenith, the satellite zenith and the relative azimuth angles (between the Sun and satellite), respectively. To avoid contamination arising from glint, we do not retrieve aerosol properties from boxes within 40° of the specular reflection angle.

[19] *Remer et al.* [2002] has shown that as compared with oceanic AERONET Sun photometer data, the ocean algorithm gives optical depth accuracy of $\Delta\tau = \pm 0.03\tau \pm 0.05$. For the effective radius, the accuracy was calculated to be ±0.10 μm. However, all of their validation points were of nondust aerosol.

2.3. PRIDE Data

[20] Table 2 lists the date and time of each MODIS overpass over Roosevelt Roads, Puerto Rico during PRIDE. Included are data for the solar and satellite zenith angles and the relative azimuth angle between the two (all measured from the surface). The next columns define the path scattering angle, and the computed glint angle (from equation 6). The last column denotes whether Roosevelt Roads is within the defined glint masked region (less than 40° from the specular angle). Note that MODIS does not operationally retrieve aerosol properties over the ocean for "Glint" overpasses.

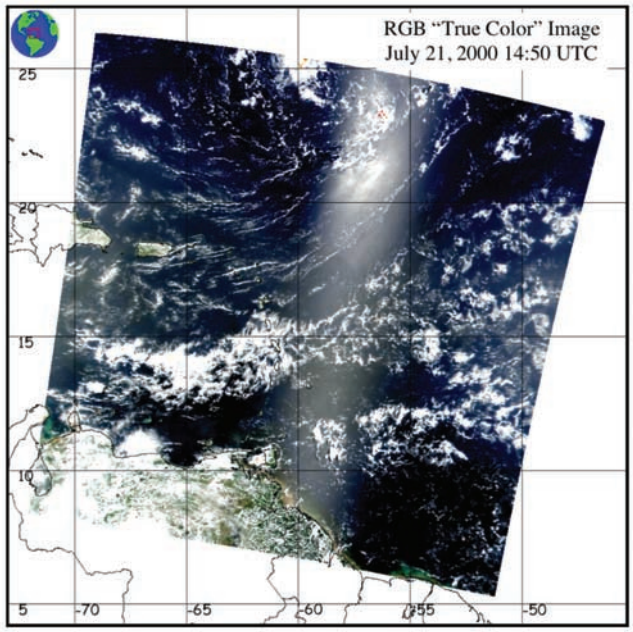

Figure 1. MODIS "true-color" imagery seen on 21 July 2000. The image is a composite of red green and blue MODIS channels. Note Puerto Rico to the left of center, and the glint reflection visible in the upper middle of the image.

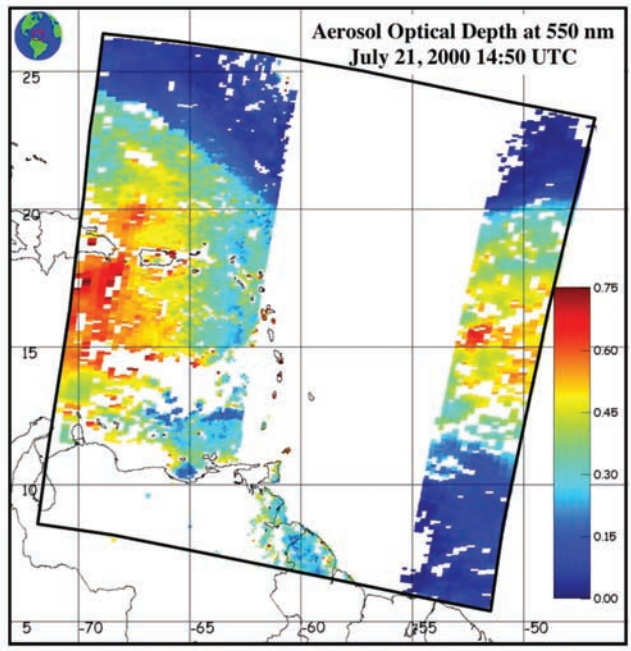

Figure 2. MODIS combined land and ocean Optical Depth retrieval (at 550 nm) for 21 July 2000. Notice Puerto Rico to the left of the center. The operational glint mask removes areas within 40° of the specular reflection angle.

[21] Some of the higher optical depth conditions during PRIDE occurred on 21 July 2000 (Julian day 203), when the optical depth at 0.55μm was about 0.5. Figure 1 shows the MODIS "true-color" image, produced by combining reflectance data from the MODIS red, green and blue channels (0.66, 0.55, and 0.47 μm). In the image, Puerto Rico (at 18°N, 66°W) is located about one third of the way between the left and right sides, approximately centered vertically. Notice the glint visible near the top of the image.

[22] Figure 2 is the corresponding MODIS aerosol retrieval at 0.55 μm for the image in Figure 1, combined for land and ocean. The potential "glint" region (40°) is masked out in gray, along with areas removed by the cloud mask. This 40° glint mask is purposely conservative, and encompasses a much larger area than the area anticipated by the visible glint in Figure 1. Also, some of the glint may not be visible in Figure 1 because it is obscured by heavy dust. At the time this data was acquired, the main pulse of the high optical depth was near or slightly west of Puerto Rico. To the east of the "glint" mask, we see evidence of the moderate dust plume that hit Puerto Rico a few days later.

3. Validation Data Sets

[23] To validate MODIS data, we employed data from multiple instrument platforms. For direct comparison of optical depth, we used three different types of Sun photometers. By using both AERONET Sun photometer almucantars and ground-based in situ retrievals, we could investigate the accuracy of MODIS size distribution retrievals. As a schematic illustration, Figure 3 shows where instruments were deployed in relation to the MODIS satellite track on 4 July 2000.

3.1. Sun Photometer Data

[24] For the validation of MODIS optical depth, we used data collected from three types of Sun photometer instruments. Two automatic Sun photometers were provided by

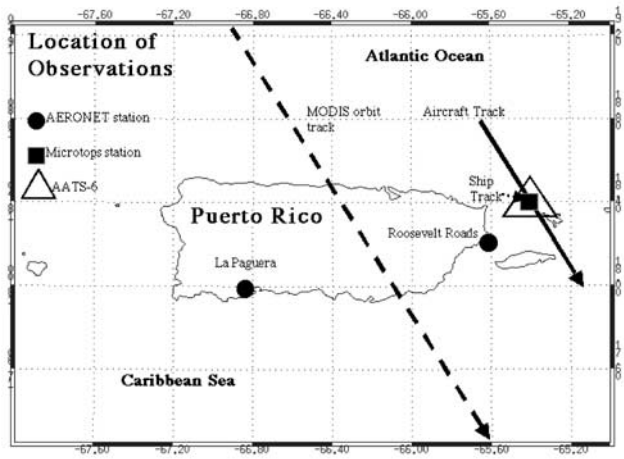

Figure 3. Schematic showing how the field instruments were deployed together on 4–6 July, where the solid circles, solid square, and open triangle represent approximate locations of the AERONET, MICROTOPS, and Ames Sun photometers. The solid line is a flight track of the Navajo aircraft, following the same heading as the MODIS satellite track (dotted). In situ data were taken at Roosevelt Roads.

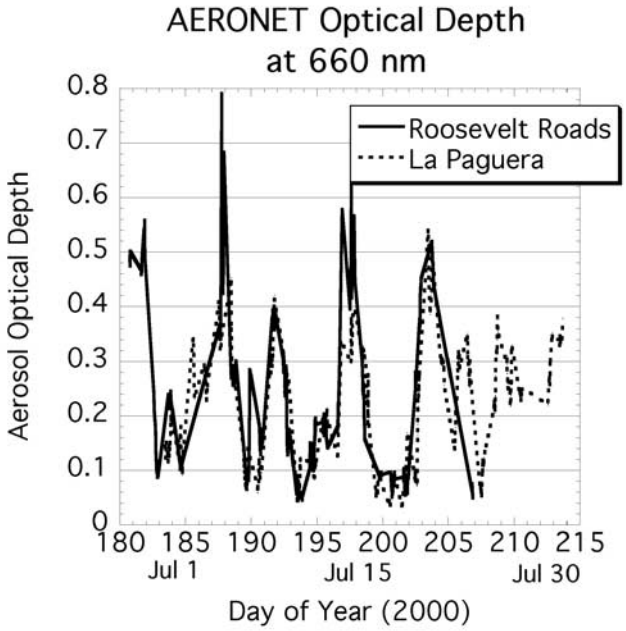

Figure 4. Time series of columnar optical depth from Roosevelt Roads and La Paguera AERONET stations during PRIDE. Day 183 corresponds to 1 July 2000.

the AERONET program [*Holben et al.*, 1998] for the duration of PRIDE. Two MICROTOPS II handheld Sun photometers [*Morys et al.*, 2001] were deployed at various times and locations, including during ship cruises. Finally, the 6 channel Ames Airborne Tracking Sunphotometer (AATS-6) [*Matsumoto et al.*, 1987] was flown aboard the Navajo aircraft on numerous flights [*Livingston et al.*, 2003]. On different days, measurements from some or all of the Sun photometers coincided with MODIS overpass. Spectral ranges are 0.44–1.02 μm for AERONET, 0.34–0.87 μm for MICROTOPS and 0.38–1.02 μm for the AATS-6.

3.1.1. AERONET Sun/Sky Photometers

[25] The AERONET network is a global network of Sun/sky autonomous radiometers. Description of the instruments and data acquisition is given by *Holben et al.* [1998]. In "Sun" mode, the instrument automatically tracks the Sun, retrieving optical depth inferred from measurements of solar extinction. In "sky" mode, the instrument measures radiance in the Sun's almucantar (same zenith angle, varying azimuth), which are later used to retrieve aerosol size distribution and other parameters.

[26] Two such instruments were deployed for the duration of the PRIDE experiment, one along the east coast of Puerto Rico at Roosevelt Roads (Latitude = 18.20°N, Longitude = 65.60°W) the other along the south coast in La Paguera (Latitude = 17.97°N, Longitude = 67.05°W). These instruments (especially Roosevelt Roads) were expected to measure dust directly transported over the ocean, with little contamination from other sources.

[27] During PRIDE, both instruments performed sky and Sun measurements in at least four spectral bands (0.44 μm, 0.67 μm, 0.87 μm and 1.02 μm), from which the aerosol optical depth and the aerosol size distribution were derived. Direct optical depth measurements were taken approximately every 15 minutes, while sky radiance data were observed every hour. Figure 4 presents a time series of PRIDE optical depth at both Roosevelt Roads and La Paguera. Optical depth calibrations are based on intercomparison with a reference instrument (usually one calibrated at the pristine mountain top of Mauna Loa, in Hilo, Hawaii), whereas radiance measurements are calibrated using an integrating sphere at NASA-Goddard Space Flight Center. Expected errors are less than 0.01 for the optical depth, and less than 5% for the sky radiance [*Holben et al.*, 1998].

[28] All direct optical depth measurements have been quality checked and cloud screened using the method of *Smirnov et al.* [2000a]. Sufficiently symmetric almucantar radiance measurements were turned into retrievals of aerosol size distribution by the method of *Dubovik and King* [2000]. The third column of Table 3 lists almucantars taken within two hours of MODIS overpass.

3.1.2. Handheld Sun Photometers

[29] Two handheld Sun photometers (MICROTOPS II) were deployed for PRIDE. These instruments, manufactured by Solar Light Co, Inc (Philadelphia, PA USA), weigh less than a kilogram and measure 10 × 20 × 4.3 cm [*Morys et al.*, 2001]. Both of our instruments were identical, intended to measure AOD at four channels (0.340, 0.440, 0.675 and 0.870 μm) and the precipitable water column using 0.936 μm.Calibration for these instruments was done from intercomparison with a reference Sun photometer [*Ichoku et al.*, 2002b]. Usually this instrument was a reference AERONET instrument located at Goddard Space Flight Center (regularly calibrated by performing Langley plot analyses at the pristine Mauna Loa Observatory in Hawaii). Calibration error for MICROTOPS optical depth is no more than 0.02 [*Ichoku et al.*, 2002b].

[30] Tests show that two main sources of error are improper pointing at the Sun, and improper cloud screening decisions [*Ichoku et al.*, 2002b]. In practice, users of these handheld Sun photometers undergo proper orientation before use, in order to minimize these and other errors. Even so, we require three or more scans in quick succession, per observation, and retain only those triplets that are sufficiently constant in value.

[31] These instruments are highly portable and can be deployed at locations where the logistics of installing other types of Sun photometers may be impossible. During one three day period, intensive observations were taken aboard the University of Puerto Rico's RV Chapman, at various ocean locations east of Puerto Rico. We learned that taking measurements aboard a rolling ship causes unique problems for Sun-pointing, but we believe that taking multiple scans per observation enabled quality control. The fourth column in Table 3 lists the dates and location of calibrated MICROTOPS measurements, corresponding to MODIS overpass. Observations labeled "Roosy Roads" were taken at several locations, but always within a few kilometers of the AERONET Sun photometer at Roosevelt Roads.

3.1.3. Ames Airborne Tracking Sunphotometer

[32] The Ames Airborne Tracking Sunphotometer automatically tracks the Sun and measures the transmitted solar beam, retrieving the overlying columnar optical depth [*Russell et al.*, 1993; *Matsumoto et al.*, 1987]. During PRIDE, the 6-channel version was mounted in the Navajo aircraft and was set to observe AOD and column water vapor. It measured direct solar beam transmission in six spectral

Table 3. Identification of Ground-Based and Airborne Aerosol Measurements Coincident With MODIS Overpass[a]

Date	MODIS Time, UTC	G/NG	AERONET Almucanturs Location, Time (UTC)	MICROTOPS (Latitude, Longitude), Location	AATS (Latitude, Longitude)	In Situ
26 June 2000	14:58	NG				
27 June 2000	15:41	G				
28 June 2000	14:46	NG				
29 June 2000	15:29	G				
30 June 2000	14:34	NG	RR 14:27			
1 July 2000	15:16	G				
2 July 2000	15:59	NG				
3 July 2000	15:04	NG				Y
4 July 2000	15:47	NG		(17.961, −64.961), Chapman	(17.93, −64.97)	Y
5 July 2000	14:52	NG		(18.167, −64.833), Chapman		Y
6 July 2000	15:34	G		(18.583, −65.167), Chapman		Y
7 July 2000	14:39	NG	RR 14:29, 15:29	(18.250, −65.633), Roosy		Y
8 July 2000	15:22	G				Y
9 July 2000	16:04	NG	LP 14:35	(18.250, −65.633), Roosy		Y
10 July 2000	15:10	G	LP 14:35	(18.224, −65.646), Roosy	(18.47, −65.15)	Y
11 July 2000	15:52	NG		(18.224, −65.646), Roosy	(18.56, −65.41)	Y
12 July 2000	14:57	NG		(18.224, −65.646), Roosy	(17.33, −65.43)	Y
13 July 2000	15:40	G		(18.224, −65.646), Roosy	(18.96, −65.13)	Y
14 July 2000	14:45	NG				Y
15 July 2000	15:28	G				
16 July 2000	14:33	NG	RR 14:30, 15:30	(18.224, −65.646), Roosy		Y
17 July 2000	15:15	G		(17.939, −67.017), one day cruise		Y
18 July 2000	15:58	NG		(18.224, −65.646), Roosy		
19 July 2000	15:02	NG	RR 14:30,15:30; LP 14:36	(18.224, −65.646), Roosy	(18.24, −65.47)	
20 July 2000	15:46	NG			(17.58, −65.96)	
21 July 2000	14:50	NG			(17.98, −65.65)	
22 July 2000	15:33	G				
23 July 2000	14:38	NG			(17.92, −65.38)	
24 July 2000	15:21	G				
25 July 2000	16:03	NG				
26 July 2000	15:09	G				

[a]The column marked "G/NG" refers to whether Roosevelt Roads was within the MODIS glint mask. The listing for AERONET is for almucantars taken within two hours of overpass. For the MICROTOPS, the location (and name of location) is exactly at overpass, while for the AATS-6, the location is the midpoint of its low-level leg. The last column denotes in situ measurements within one hour of overpass.

channels (380.1, 450.9, 525.7, 864.5, 941.9, and 1021.3 nm, with filter bandwidths of 5.0–5.8 nm) [*Livingston et al.*, 2003]. Data were digitized and recorded every 3 seconds.

[33] The AATS-6 was calibrated before and after PRIDE, by taking it to the pristine conditions of the Mauna Loa Observatory, Hawaii, and performing Langley plot analyses [*Russell et al.*, 1993]. AATS-6 data quality during PRIDE are discussed by *Livingston et al.* [2003].

[34] During PRIDE, the Navajo flight paths were designed in part so that the AATS-6 could measure the vertical distribution of AOD. However, most flights included a level track within 100 m of the ocean surface, between 5 minutes before and 5 minutes after MODIS overpass. Calculations from near-surface extinction measurements, as well as comparisons between AERONET and AATS-6 during low-altitude flights over Roosevelt Roads, show that AOD below the aircraft (0.001–0.003) were negligible compared to the instruments' uncertainties (0.01–0.02) [*Livingston et al.*, 2003]. We therefore applied no correction to the AATS-6 low-altitude (<100 m) AODs before comparing them to the MODIS data. The fifth column of Table 3 lists the AATS-6 flights during PRIDE, where the latitude and longitude values are the midpoint of the near-surface flight track.

3.2. In Situ Measurements

[35] During PRIDE, ground based aerosol sampling and in situ optical measurements were made at Roosevelt Roads. The instrumentation and setup were similar to that described by *Maring et al.* [2000]; however, here we will only describe them briefly.

[36] A sample intake pipe brought air from the roof of the trailer laboratory down to an instrument table. Just above the table, the pipe made a 90° bend and ran horizontally to provide sample air to the instruments. At certain points, smaller tubes were connected such that the original air sample was teed off to different instruments. This intake quantitatively samples aerosols (less than 10% error) for up to 10 μm diameter (5 μm radius; hereafter, we will denote size in terms of radius), but has up to 50% error for larger particles. The lowest meter of the tube includes an inline heater to control the relative humidity of the sample. The total flow rate in the intake was set to 90 L min^{-1}, which provided a laminar flow such that diffusional losses for 3 nm particles were less than 4%.

[37] Aerosol number size distributions were measured with a series of instruments. A TSI® Aerodynamic Particle Sizer (APS) Model APS33 measured large aerosols from 0.4 to >7.5 μm aerodynamic radius with a resolution of 32 channels per half decade. Smaller particles (0.075 to 0.425 μm) were measured by a TSI® Scanning Mobility Particle Sizer (SMPS) Model 3934L. Corrections to the aerosol size distributions, for aerodynamic and diffusional loss, are discussed by *Maring et al.* [2000]. The combined information from these instruments give aerosol number size distribution in 150 radius bins ranging from about

0.007 μm to 7 μm, during a twenty minute measurement. From the size distribution, we can calculate a particle effective radius (equation 5) in order to compare to MODIS.

[38] Aerosol light scattering measurements were performed using a TSI® integrating Nephelometer Model 3563 [*Anderson et al.*, 1996]. The instrument measures total and backscattering by aerosols at 0.45, 0.55 and 0.70 μm. Data were corrected for angular nonidealities according to *Anderson and Ogren* [1998]. Data were recorded as five minute averages during the period 2 to 24 July.

[39] Nearly continuous measurements by both sets of instruments were made during PRIDE. The data we use from the Particle Sizers were from the twenty minute measurements taken between ±1 hour of MODIS overpass, daily for the period 3 July to 14 July and 16 July to 18 July (there were instrument problems on 15 July and after 18 July). The nephelometer data used also correspond to the same overpass time windows (but including 15 July and 18–24 July).

4. Validation of MODIS Retrievals

[40] By deploying multiple instruments at different locations, we had a better chance of catching a comparison to MODIS. Also, more comprehensive studies of aerosol properties could be performed. Because data from each validating instrument were taken at different frequencies, slightly different approaches are used to compare MODIS with each data set.

[41] To compare MODIS optical depth with ground Sun photometer data, we use the spatiotemporal approach outlined by *Ichoku et al.* [2002a], where the main assumption is that spatial statistics from satellite retrievals can be compared to temporal statistics from point observations. According to in situ data taken at Roosevelt Roads, the average wind speed within ±1 hour of satellite overpass was similar to the 6.0 m/s used in the lookup tables (average = 5.98 m/s, standard deviation = 0.82 m/s). If we assume that the parcel can travel in any direction, aerosol can travel up to 22 km in any direction within an hour. For easier computations, we chose a 50 km by 50 km grid as our MODIS validation box. That is, each validation box is composed of five 10 km × 10 km MODIS aerosol retrieval pixels in each direction (25 total).

[42] For the Sun photometer direct Sun measurement data, we counted all valid observations within ±30 minutes of MODIS overpass. For both MODIS and ground-based measurements, we computed statistics for comparable quantities. Acceptable comparisons were defined when aerosol was retrieved in at least 20% of the pixels (i.e., five 10 km × 10 km pixels out of a possible 25) and at least two valid Sun photometer retrievals (out of a possible four or five for AERONET, and more for other types).

[43] When comparing size distribution retrievals, we were less stringent. Because only one almucantar was performed per hour, we could not usually expect to get two almucantars within the one hour period. Therefore we relaxed to allow a single valid AERONET retrieval within a two hour period (±1 hour of overpass). For comparisons with in situ scattering and aerosol size parameters, we also used averages taken about ±1 hour of MODIS overpass.

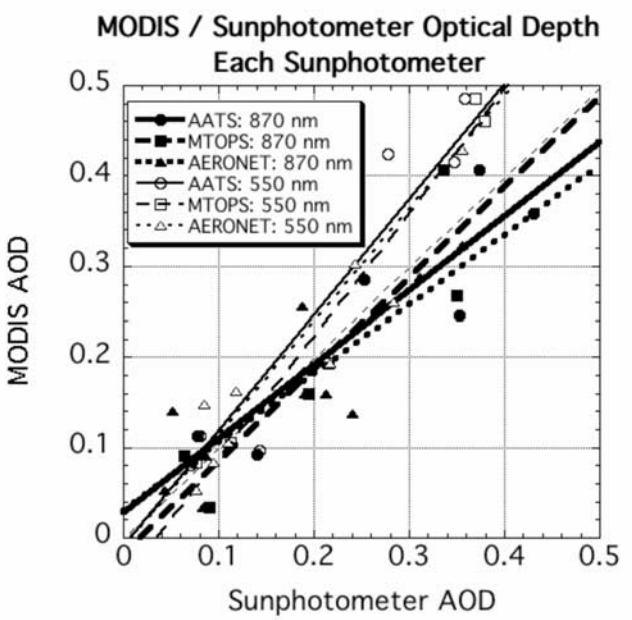

Figure 5. Spatiotemporal comparison of MODIS optical depth retrievals (for 870 nm and 550 nm) for each of the Sun photometers (AERONET, MICROTOPS, and AATS) used during PRIDE. Lines represent linear regression by wavelength for each Sun photometer. The thin dashed line is the one-to-one line for comparison.

However, we still used the 50 km × 50 km box for MODIS.

4.1. Aerosol Optical Depth

[44] Total aerosol column optical depth at a particular wavelength, τ_λ, is the quantity most easily "validated." Figure 5 shows optical depth of MODIS compared to Sun photometer for two wavelengths (0.87 and 0.55 μm), separated by Sun photometer type (AERONET, MICROTOPS and AATS). Only at the 0.87 μm channel, can MODIS be directly compared with all three Sun photometers. At 0.55 μm, linear interpolation in log/log space was performed (between 0.50 and 0.67 μm for AERONET, between 0.440 and 0.675 μm for Microtops and between 0.525 and 0.864 μm for the AATS). The lines are linear regression fits. We see that, for a given wavelength, there are no systematic differences between fits for different Sun photometers, implying that all Sun photometer data can be grouped together.

[45] Now combining the data from all three Sun photometers into one data set, we colocate and compare aerosol optical depth at 0.87, 0.66, and 0.47 μm (Figure 6). For each point, standard deviation for MODIS is plotted vertically, and represents the spatial standard deviation of optical depth within the 50 × 50 km box. Standard deviation for the Sun photometers, representing the temporal standard deviation within the one hour period, is plotted horizontally, We see that in general, the standard deviations are comparable in magnitude. Regression lines are given for each wavelength, and we notice that for all three wavelengths, the magnitude of the y-intercept is less than 0.04, implying little or no surface contamination to the retrievals. Both the 0.87 and 0.66 μm regression lines lie within the expected retrieval error over ocean ($\Delta\tau = \pm 0.03 \pm 0.05\tau$; thin lines), defined by *Remer et*

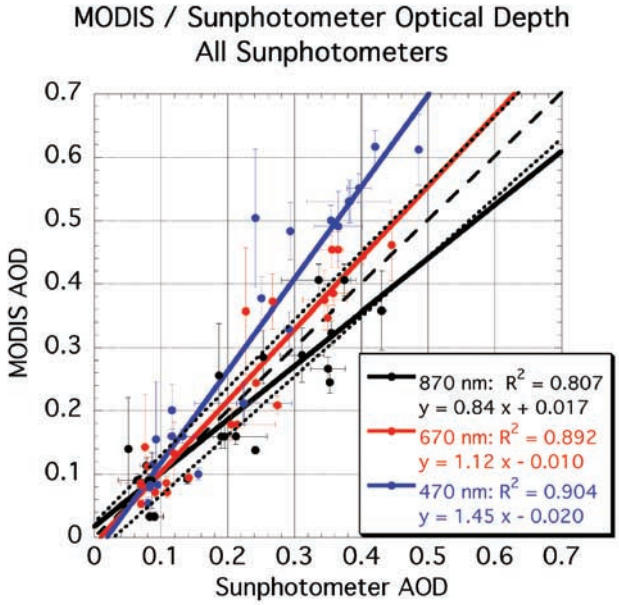

Figure 6. Spatiotemporal comparison of MODIS optical depth retrievals for all Sun photometers grouped together. Blue, red, and black lines are linear regressions for blue, red, and IR wavelengths, respectively. The thin dotted black lines are the expected errors ($\pm 0.03 \pm 0.05\tau$) published by *Remer* [2002], and the thin dashed line is the one-to-one line. The vertical error bars represent spatial standard deviation from MODIS AOD retrievals within the 50 km box, while the horizontal error bars are temporal standard deviations from the Sun photometers.

al. [2002]. However, the 0.47 μm line lies outside (overprediction by MODIS). Over all, we see that from long to short wavelengths (0.87 μm to 0.66 μm to 0.47 μm), MODIS goes from under-predicting to overpredicting the AOD.

4.2. Ångstrom Exponent and Spectral Dependence of AOT

[46] A parameter used to analyze the dependence of the optical depth on wavelength is the Ångstrom exponent, α, defined as:

$$\alpha_{\lambda_1,\lambda_2} = -\frac{\ln(\tau_{\lambda_1}/\tau_{\lambda_2})}{\ln(\lambda_1/\lambda_2)} \quad (7)$$

where τ is the optical depth at wavelengths λ_1 and λ_2 [*Eck et al.*, 1999]. Figure 7 plots the Ångstrom exponent calculated from 0.66 and 0.47 μm for MODIS versus that for the Sun photometers. Only the Ångstrom exponents for optical thickness (at 0.66 μm) greater than 0.15 are plotted, because at low optical thickness a small optical depth error at one or both wavelengths can introduce huge errors to the Ångstrom exponent (as seen by *Ignatov et al.* [1998]). Yet, MODIS consistently overpredicts the Ångstrom exponent. Also plotted in Figure 7 is a comparison of MODIS compared with an in situ scattering estimate of Ångstrom exponent. While this is only a single point (16 July), and it is at slightly different wavelengths, it is consistent compared to the Sun photometer retrievals. All MODIS Ångstrom exponent values lie above the one to one line.

[47] Another way of looking at the AOD spectral dependence is to compare MODIS optical depth retrieval to Sun photometer retrieval, plotted in wavelength space. Figure 8 shows the spectral dependence of each retrieval for cases with τ_{660} greater than 0.15. For the same color curves, the solid curve connects the Sun photometer data, while the dotted curve connects MODIS AOD. On two dates, coincident Sun photometer measurements were made during MODIS overpass. On 16 July, Roosevelt Roads (AERONET) and Roosey Roads (MICROTOPS) were operated next to each other, and observed nearly identical spectral optical thickness (red and pink curves). On 4 July, the AATS flew directly above the ship borne MICROTOPS, and observed similar optical depths in the red and near IR wavelengths, but varied somewhat at other wavelengths (dark and light green curves). For each of these pairs, there is only a single MODIS retrieval. The MODIS AOD retrievals display large spectral dependence as compared to the Sun photometer retrievals.

4.3. Aerosol Size Parameters

[48] The Ångstrom exponent, a measure of the spectral dependence of aerosol optical depth, is related to the size distribution of the measured particles. Small Ångstrom exponent values are associated with large particles in accordance with Mie scattering theory. The fact that MODIS overpredicts the wavelength dependence of optical depth, means that it will under-predict the size distribution. Figure 9 displays a comparison of the AERONET and MODIS effective radii (dots) calculated from equation 5.

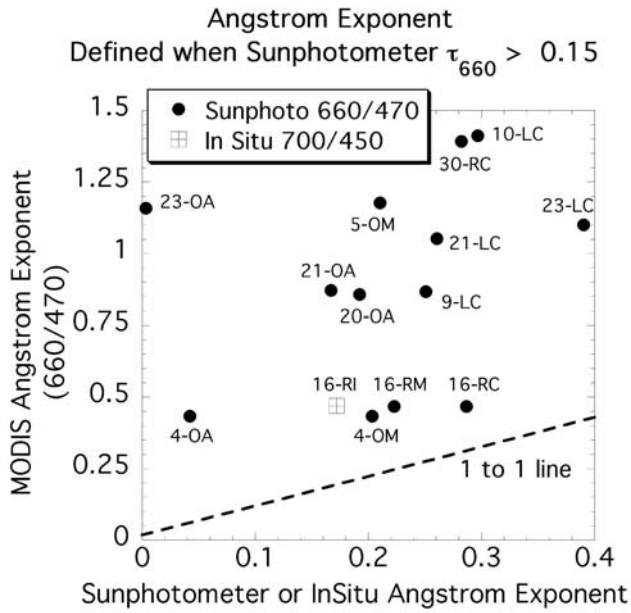

Figure 7. Comparison of MODIS Ångstrom exponent to Sun photometer (dots) and to in situ nephelometer measurements (square), showing that MODIS overpredicts for all cases (compared to the dotted one-to-one line). The text associated with each symbol represents the day of July (except 30 = 30 June), location and type of instrument. Locations: R, Roosevelt Roads; L, La Paguera; O, ocean. Instruments: C, Cimel (AERONET); M, MICROTOPS; A, AATS-6; I, in situ.

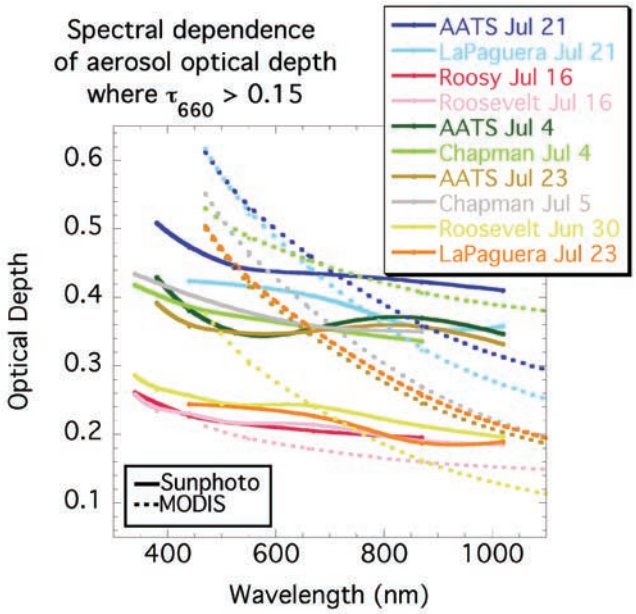

Figure 8. Spectral dependence of PRIDE optical depth, when Sun photometer $\tau_{670} > 0.15$. For the same color curves, solid curves connect Sun photometer measurements, while dotted curves connect MODIS retrievals. Measurements from the same date are similar in color (i.e., light blue and dark blue for 21 July). Roosevelt Roads (AERONET) and Roosey Roads (MICROTOPS) were operated next to each other on 16 July, and the AATS flew directly above the RV Chapman (MICROTOPS) on 4 July. Because each of these pairs of Sun photomer measurements occurred in the same MODIS "pixel," only one MODIS retrieval is associated with each pair.

Each point represents a successful sky radiance inversion from within two hours of MODIS overpass. When there were two retrievals (one before overpass, one after), they are marked with "A" and "B." Note that there are fewer points plotted than for direct optical depth comparisons, because size distribution retrievals are only possible from AERONET data. The actual optical depth (magnitude is represented by the "error bar" lines attached to each point) shows little influence upon the quality of the retrieval. During PRIDE, all values of effective radius from MODIS are far lower than corresponding values from AERONET.

[49] As for the in situ measurements of size at the surface, there are only two measurements that were coincident with MODIS overpass: 7 July and 16 July. Included on Figure 9 are the effective radii computed from the in situ size distribution (squares). Because surface dust measurements are related to total column measurements in the Caribbean [*Smirnov et al.*, 2001a], we can plot the in situ measurements on the same graph with the total column measurements. Like AERONET effective radius, they are larger than MODIS, though somewhat closer.

4.4. Validation Quality

[50] Deeper analysis of the MODIS retrieval errors yields interesting relationships. We can summarize the previous plots by stating that the accuracy of optical depth retrieval is a function of wavelength, and that the spectral error gives rise (through Mie theory) to under-prediction of the particles' size. Let us define an optical thickness error that is the departure from the expected errors ($\Delta\tau = \pm 0.03 \pm 0.05\tau$) defined by *Remer et al.* [2002]. Thus we are defining a measure that works for all values of optical depth, encompassing both the absolute error,

$$\tau_{\text{error}}^{\text{absolute}} = (\tau_{\text{MODIS}} - \tau_{\text{SP}}) \tag{8}$$

and the relative error,

$$\tau_{\text{error}}^{\text{relative}} = (\tau_{\text{MODIS}} - \tau_{\text{SP}})/\tau_{\text{SP}}, \tag{9}$$

This "expectation error" can be defined as:

$$\tau_{\text{error}}^{\text{expect}} = \frac{(\tau_{\text{MODIS}} - \tau_{\text{SP}})}{(0.03 + 0.05\tau_{\text{SP}})}, \tag{10}$$

where τ_{SP} is from a Sun photometer direct Sun measurement. By defining this measure of the error, we can define a "large" expectation error when the magnitude is greater than unity, meaning that the actual error exceeded the expected uncertainty. Because we do not yet have an expectation of the effective radius error, we will define the effective radius error simply as the relative error, that is:

$$\text{Reff}_{\text{error}}^{\text{relative}} = (\text{Reff}_{\text{MODIS}} - \text{Reff}_{\text{AERONET}}) \quad /\text{Reff}_{\text{AERONET}}, \tag{11}$$

where $\text{Reff}_{\text{AERONET}}$ is retrieved from AERONET almucantar sky measurements [*Dubovik and King*, 2000].

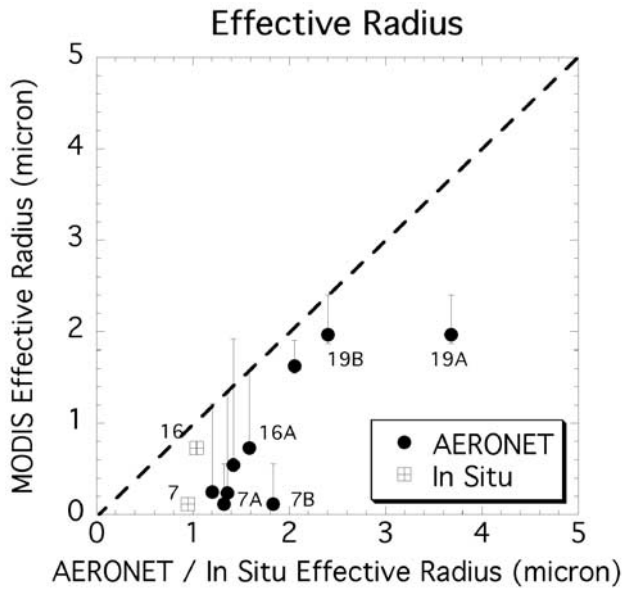

Figure 9. Comparison of effective radius retrieved from MODIS versus AERONET (dots) and in situ data at the surface (squares). The magnitude of each "error bar" is the optical depth (multiplied by 0.025). The numbers represent the date in July (e.g., 4 = 4 July), and if followed by a letter, then it represents AERONET retrieval for the same date (e.g., "A" and "B" are two almucantars within one hour of MODIS overpass). The line is one to one.

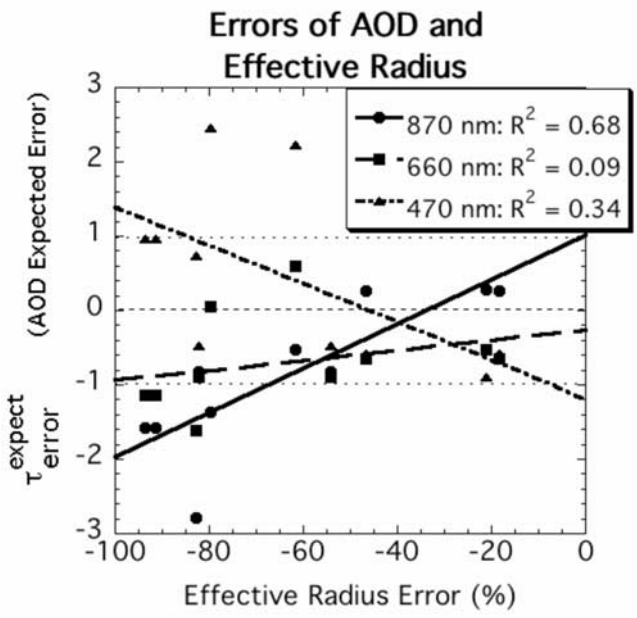

Figure 10. Relationship between effective radius error and the optical depth expectation error (defined by equation 8) for three wavelengths. Optical depth expectation error is defined so that a magnitude less than one (between thin lines at 1 and-1) represents a retrieval within the *Remer et al.* [2002] expected retrieval error ($\pm 0.03 \pm 0.05\tau$). A perfect AOD retrieval would lie on the zero line. The effective radius error is the relative error defined by equation 11.

[51] In Figure 10 these two quantities are plotted against each other for three wavelengths. Only those points having a retrieved effective radius are plotted. Note that MODIS underestimates Reff for all observations and $\text{Reff}_{\text{error}}^{\text{relative}}$ (the x axis of Figure 10) is always negative. Thus small errors in Reff are located to the right of the graph, becoming more and more negative (more severe) as they more toward the plot's left-hand edge. We see a possible relationship between error in optical thickness $\tau_{\text{error}}^{\text{expect}}$ and error in effective radius $\text{Reff}_{\text{error}}^{\text{relative}}$ that is dependent on wavelength. The greatest overestimation of optical depth at 0.47 μm, and the greatest under-estimation of optical depths at 0.66 and 0.87 μm occur when the error in Reff is most negative.

[52] Even when all wavelengths of AOD retrieval fall within expectations, we still may have errors in effective radius. This is in contrast to the nondust findings by *Remer et al.* [2002] that MODIS effective radii differed from AERONET values by only ±0.1 μm. These wavelength dependence and effective radius retrieval problems seem to be unique to the dusty conditions during PRIDE.

5. Discussion and Further Study

[53] For PRIDE, we have compared MODIS aerosol retrievals over ocean with optical depth and aerosol size retrievals from Sun photometers. Regression lines of MODIS retrievals of optical depth (compared with Sun photometers) fall mostly within published estimates [*Remer et al.*, 2002] at both 0.87 and 0.66 μm, but at 0.87 μm are somewhat underestimated. At 0.47 μm, MODIS significantly overestimates the optical depth. Following the spectral AOD discrepancies, MODIS retrieves small mode particles in dust regions, where we believe large particles dominate. We anticipated these spectral AOD and size discrepancies when we assumed simplified spherical aerosol models in the original MODIS algorithms.

[54] According to *Dubovik et al.* [2000, 2002], nonsphericity of dust particles can cause retrieval of a "spurious" small mode in the AERONET retrievals, especially when using radiance from scattering angles greater than 45°. The actual dust phase function better resembles phase functions of smaller spherical particles than phase functions from spherical particles having dust size [*Mischenko and Travis*, 1997]. Figure 11 shows the size distributions retrieved from AERONET for almucantars within two hours of MODIS overpass. Nearly all of these almucantars occur around 14:30 UTC (10:30 AM local Puerto Rico time), corresponding to a solar zenith angle around 27° (see Table 2, 16 July entry) implying almucantar scattering angles up to 52°. The associated retrievals show a mode centered around 0.1 μm, which would be nonphysical [*Dubovik et al.*, 2000, 2002].

[55] This brings up an interesting observation. That is, if the AERONET has a spurious small mode, then the effective radius computed from AERONET is already too small. This implies that the even smaller effective radii retrieved from MODIS are actually worse. The in situ size measurements also suggest that MODIS retrievals may be far too small. The two squares plotted in Figure 9 are reasonably close to the one-to-one line. However, literature [*Maring et al.*, 2000] tells us that the Particle Sizers may under-sample the large particles (up to 50% for 10 μm particles) so that in reality, the in situ effective radius would be larger. It is interesting to note that all three types of measurements seem to under-estimate particle size.

[56] According to *Mischenko and Travis* [1997], large scattering angles magnify optical differences between

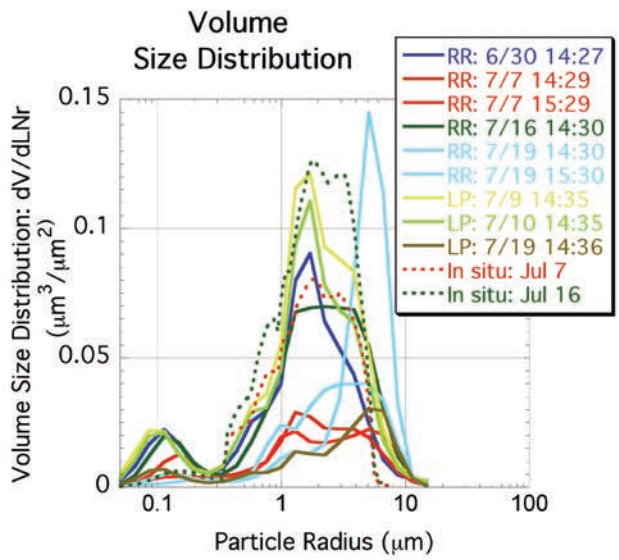

Figure 11. Volume size distribution retrieved from AERONET almucantars (solid curves) and from in situ data (dotted curves), corresponding to valid MODIS retrievals. For in situ data we are assuming an aerosol layer thickness of 1 km, to derive the same units.

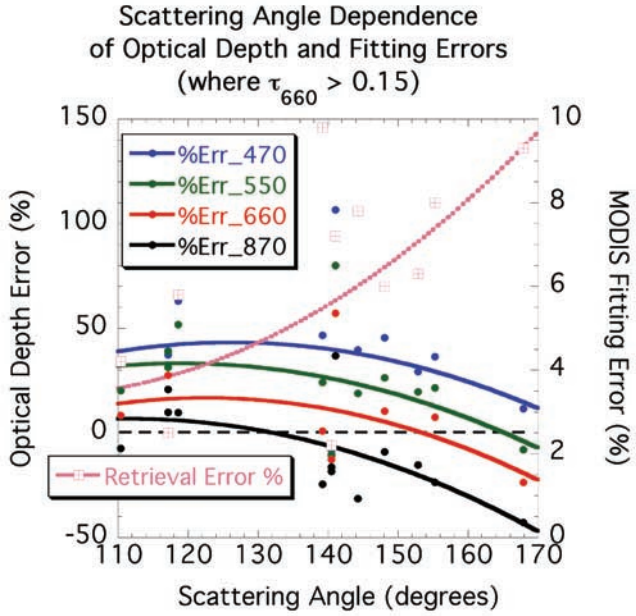

Figure 12. Optical depth error (in percent) compared with scattering angle for four MODIS wavelengths (blue, green, red, and IR). MODIS reflectance fitting error is given by the crosses. The curves are second-order polynomials.

spheres and nonspheres. Therefore for MODIS data, where scattering angles are all very large, we might expect to see some dependence of the retrieval upon scattering angle. Figure 12 shows errors of the spectral optical depth and reflectance fitting, against scattering angle (for $\tau_{660} > 0.15$). Because the optical depth is large enough, we use the relative optical depth error, defined as equation 9 and the reflectance fitting error defined by equation (4) in section 2. The curves are fits to the data using second-order polynomials. For all four wavelengths, the optical depth error is nearly constant up to a scattering angle of about 130°. Then MODIS tends toward under-estimation of optical depth (especially at 0.87 μm) as the scattering angle increases. We also see that as the scattering angle increases, MODIS has more difficulty fitting the modeled reflectance to the observed reflectance. These trends, as functions of scattering angle, suggest problems with our aerosol model for dust-like aerosols. Problems could include our assumptions of size distribution and/or our assumptions about refractive indices. However, given the AERONET experience, errors are most likely due to assumptions of spherical particles, and the use of Mie theory in construction of the MODIS lookup tables.

[57] PRIDE was our first opportunity to evaluate the performance of MODIS in dust settings. The PRIDE results tell us that errors in the retrieval, including the anticipated errors introduced by nonsphercity, do not appear to significantly degrade our optical depth retrievals at 0.87 and 0.66 μm. However, problems with the dust aerosol model, which may be due to nonsphericity, do appear to affect optical thickness retrievals at other wavelengths and cause severe under-prediction of the dust particle size. These problems can be corrected. Over time, the growing data base of colocated MODIS retrievals and Sun photometer measurements (in dust environments), will provide us with sufficient data to measure the phase function of the ambient, column integrated, nonspherical dust at MODIS observation angles. We plan to derive empirically corrected phase functions and to introduce these into the MODIS lookup tables, such as proposed by *Ignatov* [1997]. These new lookup tables should improve the ability of MODIS to observe and monitor dust aerosol.

[58] **Acknowledgments.** We would like to thank SSAI's Richard Kleidman for installation and maintenance of the two AERONET Sun photometers, and for collection of some of the MICROTOPS data. We are thank all others whom have collected MICROTOPS data, including Roy Armstrong and Julio Morel from the University of Puerto Rico, Rick Hansel from the University of California, Los Angeles and Joe Prospero from the University of Miami. We appreciate the crew of the R/V Chapman for their assistance and accommodation. Finally, we would like to thank SSAI's Shana Mattoo for her insight and discussion about the MODIS algorithm and University of Maryland-Baltimore County's Oleg Dubovik for help with the AERONET retrievals.

References

Ahmad, Z., and R. S. Fraser, An Iterative Radiative Transfer Code For Ocean-Atmosphere Systems, *J. Atmos. Sci.*, *39*, 656–665, 1981.

Alpert, P., Y. J. Kaufman, Y. Shay-El, D. Tanré, A. da Silva, S. Schubert, and J. H. Joseph, Quantification of dust-forced heating of the lower troposphere, *Nature*, *395*, 367–370, 1998.

Anderson, T. L., and J. A. Ogren, Determining aerosol radiative properties using the TSI 3563 integrating nephelometer, *Aerosol Sci. Tecnol.*, *29*, 57–69, 1998.

Anderson, T. L., et al., Performance characteristics of a high sensitivity, three-wavelength, total scatter/backscatter nephelometer, *J. Atmos. Oceanic. Technol.*, *13*, 967–986, 1996.

Chiapello, I., J. M. Prospero, J. R. Herman, and N. C. Hsu, Detection of mineral dust over the North Atlantic Ocean and Africa with the Nimbus 7 TOMS, *J. Geophys. Res.*, *104*(D8), 9277–9291, 1999.

Cox, C., and W. Munk, Statistics of the sea surface derived from Sun glitter, *J. Mar. Res.*, *13*, 198–208, 1954.

Dickerson, R. R., S. Kondragunta, G. Stenchikov, K. L. Civerolo, B. G. Doddridge, and B. N. Holben, The impact of aerosol on solar ultraviolet radiation and photochemical smog, *Science*, *278*, 827–830, 1997.

Dubovik, O., and M. D. King, A flexible inversion algorithm for retrieval of aerosol optical properties from Sun and sky radiance measurements, *J. Geophys. Res.*, *105*(D16), 20,673–20,696, 2000.

Dubovik, O., A. Smirnov, B. N. Holben, M. D. King, Y. J. Kaufman, T. F. Eck, and I. Slutsker, Accuracy assessments of aerosol optical properties retrieved from Aerosol Robotic Network (AERONET) Sun and sky radiance measurements, *J. Geophys. Res.*, *105*(D8), 9791–9806, 2000.

Dubovik, O., B. N. Holben, T. F. Eck, A. Smirnov, Y. J. Kaufman, M. D. King, D. Tanré, and I. Slutsker, Variability of absorption and optical properties of key aerosol types observed in worldwide locations, *J. Atmos. Sci.*, *59*, 590–608, 2002.

Eck, T. F., B. N. Holben, J. S. Reid, O. Dubovik, A. Smirnov, N. T. O'Neill, I. Slutsker, and S. Kinne, Wavelength dependence of the optical depth of biomass burning, urban, and desert dust aerosols, *J. Geophys. Res.*, *104*(D24), 31,333–31,349, 1999.

Formenti, P., M. O. Andreae, L. Lange, G. Roberts, J. Cafmeyer, I. Rajta, W. Maenhaut, B. N. Holben, P. Artaxo, and J. Lelieveld, Saharan dust in Brazil and Suriname during the Large-Scale Biosphere-Atmosphere Experiment in Amazonia (LBA)-Cooperative LBA Regional Experiment (CLAIRE) in March 1998, *J. Geophys. Res.*, *106*(D14), 14,919–14,934, 2001.

Gao, Y., Y. J. Kaufman, D. Tanré, D. Kolber, and P. G. Falkowski, Seasonal distributions of aeolian iron fluxes to the global ocean, *Geophys. Res. Lett.*, *28*(1), 29–32, 2001.

Ginoux, P., M. Chin, I. Tegen, J. M. Prospero, B. Holben, O. Dubovik, and S. J. Lin, Sources and distributions of dust aerosols simulated with the GOCART model, *J. Geophys. Res.*, *106*(D17), 20,255–20,273, 2001.

Gordon, H. R., Atmospheric correction of ocean color imagery in the Earth Observing System era, *J. Geophys. Res.*, *102*(D14), 17,081–17,106, 1997.

Herman, J. R., P. K. Bhartia, O. Torres, C. Hsu, C. Seftor, and E. Celarier, Global distribution of UV-absorbing aerosols from Nimbus 7/TOMS data, *J. Geophys. Res.*, *102*(D14), 16,911–16,992, 1997.

Higurashi, A., T. Nakajima, B. N. Holben, A. Smirnov, R. Frouin, and B. Chatenet, A study of global aerosol optical climatology with two-channel AVHRR remote sensing, *J. Clim.*, *13*(12), 2011–2027, 2000.

Holben, B. N., et al., AERONET—A federated instrument network and data archive for aerosol characterization, *Remote Sens. Environ.*, *66*(1), 1–16, 1998.

Husar, R. B., J. M. Prospero, and L. L. Stowe, Characterization of tropospheric aerosols over the oceans with the NOAA advanced very high resolution radiometer optical thickness product, *J. Geophys. Res.*, *102*(D14), 16,889–16,909, 1997.

Ichoku, C., D. A. Chu, S. Mattoo, Y. J. Kaufman, L. A. Remer, D. Tanré, I. Slutsker, and B. N. Holben, A spatio-temporal approach for global validation and analysis of MODIS aerosol products, *Geophys. Res. Lett.*, *29*(12), 8006, doi:10.1029/2001GL013206, 2002a.

Ichoku, C., et al., Analysis of the performance characteristics of the five-channel Microtops II Sun photometer for measuring aerosol optical thickness and precipitable water vapor, *J. Geophys. Res.*, *107*(D13), 4179, doi:10.1029/2001JD001302, 2002b.

Ignatov, A. L., Estimation of the aerosol phase function in backscatter from simultaneous satellite and Sunphotometer measurements, *J. Appl. Meteorol.*, *36*(6), 688–694, 1997.

Ignatov, A., L. Stowe, and R. Singh, Sensitivity study of the Ångstrom exponent derived from AVHRR over oceans, *Adv. Space Res.*, *21*, 439–442, 1998.

Johansen, A. M., R. L. Siefert, and M. R. Hoffmann, Chemical composition of aerosols collected over the tropical North Atlantic Ocean, *J. Geophys. Res.*, *105*(D12), 15,277–15,312, 2000.

Kaufman, Y. J., D. Tanré, L. A. Remer, E. F. Vermote, A. Chu, and B. N. Holben, Operational remote sensing of tropospheric aerosol over land from EOS moderate resolution imaging spectroradiometer, *J. Geophys. Res.*, *102*(D14), 17,051–17,067, 1997.

Kaufman, Y. J., D. Tanré, O. Dubovik, A. Karnieli, and L. A. Remer, Absorption of sunlight by dust as inferred from satellite and ground-based remote sensing, *Geophys. Res. Lett.*, *28*(8), 1479–1482, 2001.

King, M. D., Y. J. Kaufman, W. P. Menzel, and D. Tanré, Remote-sensing of cloud, aerosol, and water-vapor properties from the Moderate Resolution Imaging Spectrometer (MODIS), *IEEE Trans. Geosci. Remote Sens.*, *30*(1), 2–27, 1992.

Koepke, P., Effective reflectance of oceanic whitecaps, *Appl. Opt.*, *23*, 1816–1823, 1984.

Koren, I., E. Ganor, and J. H. Joseph, On the relation between size and shape of desert dust aerosol, *J. Geophys. Res.*, *106*(D16), 18,047–18,054, 2001.

Levin, Z., and E. Ganor, The effects of desert particles on cloud and rain formation in the eastern Mediterranean, in *The Impact of Desert Dust Across the Mediterranean*, edited by S. Guerzoni and R. Chester, pp. 77–86, Kluwer Acad., Norwell, Mass., 1996.

Li-Jones, X., and J. M. Prospero, Variations in the size distribution of non-sea-salt sulfate aerosol in the marine boundary layer at Barbados: Impact of African dust, *J. Geophys. Res.*, *103*(D13), 16,073–16,084, 1998.

Livingston, J. M., et al., Shipboard Sunphotometer measurements of aerosol optical depth spectra and columnar water vapor during ACE-2, and comparison with selected land, ship, aircraft, and satellite measurements, *Tellus, Ser. B*, *52*(2), 594–619, 2000.

Livingston, J. M., et al., Airborne Sun photometer measurements of aerosol optical depth and columnar water vapor during the Puerto Rico Dust Experiment and comparison with land, aircraft, and satellite measurements, *J. Geophys. Res.*, *108*, doi:10.1029/2002JD02520, in press, 2003.

Maring, H., D. L. Savoie, M. A. Izaguirre, C. McCormick, R. Arimoto, J. M. Prospero, and C. Pilinis, Aerosol physical and optical properties and their relationship to aerosol composition in the free troposphere at Izana, Tenerife, Canary Islands, during July 1995, *J. Geophys. Res.*, *105*(D11), 14,677–14,700, 2000.

Martins, J. V., D. Tanré, L. Remer, Y. Kaufman, S. Mattoo, and R. Levy, MODIS cloud screening for remote sensing of aerosols over oceans using spatial variability, *Geophys. Res. Lett.*, *29*(12), 8009, doi:10.1029/2001GL013252, 2002.

Matsumoto, T., P. B. Russell, C. Mina, and W. Van Ark, Airborne tracking Sunphotometer, *J. Atmos. Oceanic Technol.*, *4*, 336–339, 1987.

Miller, R. L., and I. Tegen, Climate response to soil dust aerosols, *J. Clim.*, *11*(12), 3247–3267, 1998.

Mishchenko, M. I., and L. D. Travis, Satellite retrieval of aerosol properties over the ocean using measurements of reflected sunlight: Effect of instrumental errors and aerosol absorption, *J. Geophys. Res.*, *102*(D12), 13,543–13,553, 1997.

Morys, M., F. M. Mims III, S. Hagerup, S. E. Anderson, A. Baker, J. Kia, and T. Walkup, Design, calibration and performance of MICROTOPS II handheld ozone monitor and Sun photometer, *J. Geophys. Res. Atmos.*, *106*(D13), 14,573–14,582, 2001.

Moulin, C., F. Guillard, F. Dulac, and C. E. Lambert, Long-term daily monitoring of Saharan dust load over ocean using Meteosat ISCCP-B2 data: 2. Accuracy of the method and validation using Sun photometer measurements, *J. Geophys. Res.*, *102*(D14), 16,959–16,969, 1997.

Prospero, J. M., Saharan dust transport over the North Atlantic Ocean and Mediterranean: And overview, in *The Impact of Desert Dust Across the Mediterranean*, edited by S. Guerzoni and R. Chester, pp. 133–151, Kluwer Acad., Norwell, Mass., 1996.

Prospero, J. M., Long-term measurements of the transport of African mineral dust to the southeastern United States: Implications for regional air quality, *J. Geophys. Res.*, *104*(D13), 15,917–15,927, 1999.

Prospero, J. M., P. Ginoux, O. Torres, S. E. Nicholson, and T. E. Gill, Environmental characterization of global sources of atmospheric soil dust identified with the NIMBUS 7 Total Ozone Mapping Spectrometer (TOMS) absorbing aerosol product, *Rev. Geophys.*, *40*(1), 1002, doi:10.1029/2000RG000095, 2002.

Reid, J. S., et al., Puerto Rico dust experiment (PRIDE): Mission overview, *Eos Trans. AGU*, *81*(48), Fall Meet. Suppl., F42, 2000.

Reid, J. S., et al., Analysis of measurements of Saharan dust by airborne and ground-based remote sensing methods during the Puerto Rico Dust Experiment (PRIDE), *J. Geophys.*, 108, doi:10.1029/2002JD002493, in press, 2003.

Remer, L. A., Validation of MODIS aerosol retrieval over ocean, *Geophys. Res. Lett.*, *29*(12), 8008, doi:10.1029/2001GL013204, 2002.

Rosenfeld, D., Y. Rudich, and R. Lahav, Desert dust suppressing precipitation: A possible desertification feedback loop, *Proc. Natl. Acad. Sci.*, *98*(11), 5975–5980, 2001.

Russell, P. B., et al., Pinatubo and Pre-Pinatubo optical-depth spectra: Mauna Loa measurements, comparisons, inferred particle size distributions, radiatiive effects and relationship to lidar data, *J. Geophys. Res.*, *98*(D12), 22,969–22,985, 1993.

Salomonson, V. V., W. L. Barnes, P. W. Maymon, H. E. Montgomery, and H. Ostrow, MODIS: Advanced facility instrument for studies of the Earth as a system, *IEEE Trans. Geosci. Remote Sens.*, *27*, 145–153, 1989.

Smirnov, A., B. N. Holben, T. F. Eck, O. Dubovik, and I. Slutsker, Cloud-screening and quality control algorithms for the AERONET database, *Remote Sens. Environ.*, *73*(3), 337–349, 2000a.

Smirnov, A., B. N. Holben, D. Savoie, J. M. Prospero, Y. J. Kaufman, D. Tanré, T. F. Eck, and I. Slutsker, Relationship between column aerosol optical thickness and in situ ground based dust concentrations over Barbados, *Geophys. Res. Lett.*, *27*(11), 1643–1646, 2000b.

Sokolik, I. N., D. M. Winker, G. Bergametti, D. A. Gillette, G. Carmichael, Y. J. Kaufman, L. Gomes, L. Schuetz, and J. E. Penner, Introduction to special section: Outstanding problems in quantifying the radiative impacts of mineral dust, *J. Geophys. Res.*, *106*(D16), 18,015–18,027, 2001.

Stallard, R. F., Possible environmental factors underlying amphibian decline in eastern Puerto Rico: Analysis of US government data archives, *Conserv. Biol.*, *15*(4), 943–953, 2001.

Tanré, D., M. Herman, and Y. J. Kaufman, Information on aerosol size distribution contained in solar reflected spectral radiances, *J. Geophys. Res.*, *101*(D14), 19,043–19,060, 1996.

Tanré, D., Y. J. Kaufman, M. Herman, and S. Mattoo, Remote sensing of aerosol properties over oceans using the MODIS/EOS spectral radiances, *J. Geophys. Res.*, *102*(D14), 16,971–16,988, 1997.

Tanré, D., Y. J. Kaufman, B. N. Holben, B. Chatenet, A. Karnieli, F. Lavenu, L. Blarel, O. Dubovik, L. A. Remer, and A. Smirnov, Climatology of dust aerosol size distribution and optical properties derived from remotely sensed data in the solar spectrum, *J. Geophys. Res.*, *106*(D16), 18,205–18,217, 2001.

Tegen, I., and I. Fung, Contribution to the atmospheric mineral aerosol load from land-surface modification, *J. Geophys. Res.*, *100*(D9), 18,707–18,726, 1995.

Tegen, I., A. A. Lacis, and I. Fung, The influence on climate forcing of mineral aerosols from distrubed soils, *Nature*, *380*, 419–422, 1996.

B. N. Holben, Laboratory for Terrestrial Physics, NASA Goddard Space Flight Center, Greenbelt, MD 20771, USA.

C. Ichoku and R. C. Levy, Science Systems and Applications Inc., Lanham, MD 20706, USA. (levy@climate.gsfc.nasa.gov)

Y. J. Kaufman and L. A. Remer, Laboratory for Atmospheres, NASA Goddard Space Flight Center, Greenbelt, MD 20771, USA.

J. M. Livingston, SRI International, 333 Ravenswood Avenue, Menlo Park, CA 94025, USA.

H. Maring, Rosenstiel School of Marine and Atmospheric Science, University of Miami, 4600 Rickenbacker Causeway, Miami, FL 33149, USA.

P. B. Russell, NASA Ames Research Center, Moffett Field, CA 94035, USA.

D. Tanré, Laboratoire d'Optique Atmospherique, CNRS, Universite de Sciences et Techniques de Lille, 59655, Villeneuve d'Ascq cedex, France.